Biointerface Research in Applied Chemistry
Platinum Open Access Journal (ISSN: 2069-5837)

Article
Volume 11, Issue 6, 2021, 14127 - 14141
https://doi.org/10.33263/BRIAC116.1412714141

Single-sided Time Domain-Nuclear Magnetic Resonance to Study the Effect of Cell Membrane Electroporation on the Water Mobility in Vegetal Tissues

Ileana Menegazzo [1], Stefano Mammi [1], Elisabetta Sieni [2,*], Paolo Sgarbossa [3], Alessandra Bartolozzi [3], Mirto Mozzon [3], Roberta Bertani [3], Michele Forzan [3], Raji Sundararajan [4,*]

[1] Padova University, Department of Chemical Sciences via Marzolo 1, 35131 Padova, Italy
[2] Insubria University, Department of Theoretical and Applied Sciences via Dunant, 3 21100 Varese, Italy
[3] Padova University, Department of Industrial Engineering, via Marzolo, 9, 35131 Padova, Italy
[4] School of Engineering Technology, Purdue University, Knoy Hall of Technology, 401 N. Grant St. West Lafayette, IN 47907, USA
* Correspondence: elisabetta.sieni@uninsubria.it (E.S.), raji@purdue.edu (R.S.);

Scopus Author ID 7004860497
Received: 15.01.2021; Revised: 28.02.2021; Accepted: 2.03.2021; Published: 7.03.2021

Abstract: This paper presents the characteristics of potato and apple tissues, with/out electroporation, by Time Domain-Nuclear Magnetic Resonance (TD-NMR). A portable TD-NMR was used to measure the proton relaxation time, T2, and the changes in the cells due to molecular water mobility of potato tubers,-NMR to identify the modifications that occurred at the cell level involving water molecules mobility in potato tubers and apple tissues after the electroporation treatment and compared with non-electroporated ones. The comparisons with normal potato and apple tissue and preliminary measurements in bulk were performed. Samples were also analyzed in terms of conductivity of the tissue and microscopic morphology. The results indicate that the electroporation process effect is identified with a variation of the peak position in T2 distribution, associated with sub-cell modifications.

Keywords: water mobility; electroporation; vegetal tissue; potato; time domain Nuclear-Magnetic Resonance (NMR); cell membrane.

© 2021 by the authors. This article is an open-access article distributed under the terms and conditions of the Creative Commons Attribution (CC BY) license (https://creativecommons.org/licenses/by/4.0/).

1. Introduction

Electroporation involves the targeted application of high magnitude, short width electrical pulses (EP) across the cell memabrane, which causes accumulation of charges and hence enhnaces membrane voltage, *Vm*. When Vm is around 0.5 to 1V, across its 5nm thickness, there is a several-fold enhancement of electric field (100MV/cm), leading to the pore formation [1-10].

During electroporation, drug molecules can enter the cancer cells in various ways, such as diffusion, electro-osmotic, and colloid-osmotic flow [11]. The flow of light and small drug molecules due to electroporation is given by Fick's equation [12]:

$$F_S(t) = P_S x(N,T) A/2 \left(1 - \frac{Ep}{E}\right) \Delta S e^{-k(N,T)^i} (1)$$

where Fs is the flow of molecules S diffusing through the plasma membrane, Ps is the permeation coefficient of the molecule S across the membrane, x is a function, which represents the probability of (0<x<1), A is cell surface, E is the applied electric field intensity, Ep is the

threshold for permeabilization, ΔS is concentration difference of S between the cell and external medium, k is the time constant of the resealing process, and t is the time after the pulse.

The pore formation is a two-step process [13]. First, small and non-conducting hydrophobic pores form in the cell membrane. Second, these hydrophobic pores expand in size, and lipid molecules invert on the edges to create conducting hydrophilic pores. The energy of pore formation (E(r)) for both types of pores is a function of the pore radius (r) and V_m, as shown in (1) for hydrophobic and (2) for hydrophilic pores, respectively [13].

$$E(r) = 2\pi hr\sigma_0(\infty)\,[I_1(r/r_0)/I_0(r/r_0)]) - \pi a_p V_m^2 r^2 \quad (2)$$

$$E(r) = 2\pi\gamma r - \int_0^r 2\pi\Gamma(r^*)r^*dr^* + (C/r)^4 - \pi a_p V_m^2 r^2 \quad (3)$$

where h is the membrane thickness,$\sigma_0(\infty)$is a constant ($5\cdot10^{-2}$N/m), r0 is the characteristic length, I_0 and I_1 are 0^{th} and 1^{st} order modified Bessel functions, γ is the strain energy per unit length of the bilayer pore edge or perimeter, Γ is the surface energy per unit area of the intact bilayer, C is a constant ($9.67\cdot10^{-15}$J$^{1/4}$m), a_p is the property of the membrane and its aqueous environment, expressed in terms of *h* and permittivity of water (ε_w) and membrane (ε_m), as $a_p = (\varepsilon_w - \varepsilon_m)/[2h]$.

This two-step pore formation phenomenon is called electroporation, and it can enhance the uptake of external molecules up to 1000 times [14]. When electroporation is applied towards chemotherapeutics' uptake, this non-surgical procedure, known as Electrochemotherapy (ECT), is gaining momentum as an alternative to conventional therapies for advanced, inoperable, and radio- and chemo-resistant tumors of all histological types of cutaneous and subcutaneous metastases in the EU [15]. This phenomenon is evidenced by an increment of the tissue's conductivity [1, 16–18]. This technique is applied in medicine to improve the chemotherapeutic drug uptake and the food industry to treat fruits to enhance juice extraction or in low-temperature sterilization [19–25]. This technique is also used to study the effect of electrical pulses on vegetal tissues. Towards this, numerous studies have shown that Time Domain-Nuclear Magnetic Resonance (TD-NMR) is an excellent method to characterize water mobility and water distribution in food items, such as meat, fish, cheese, cereals, fruits, and vegetables, including potatoes [26–39].

The basic physical rationale behind the generation of the NMR signal is the same in all kinds of NMR instruments, and it derives from the NMR-active atomic nuclei present in the sample. Time Domain NMR applications include the measurements of the relaxation properties of protons that, after excitation by a radiofrequency pulse, return to the equilibrium condition: energy is lost to the surroundings in the form of heat (spin-lattice relaxation), and coherence among spins is also lost (spin-spin relaxation).

The 1H NMR spin-lattice (T_1) and spin-spin (T_2) relaxation times of water in vegetable tissue have been used to describe the water status. Whereas bulk water exhibits a single value for each relaxation time, water compartmentalized in subcellular structures, such as vegetable tissues, exhibits multiple relaxation time values. Water molecules or protons are in exchange among these compartments, and the exchange rates are controlled by the permeability of the membranes separating the compartments, their size, and/or by the diffusion processes of water molecules.

Whereas differences in the longitudinal relaxation times (T_1) are usually not sufficient to identify water in different compartments, differences in transverse relaxation times (T_2) are more pronounced. Moreover, the total proton NMR signal from any sample region is directly proportional to the proton density in that region, providing quantitative information about water compartmentation.

The literature reports that in vegetable cells, the mean distribution of T_2 relaxation times includes three populations, partially overlapped, associated with three proton compartments. Specifically, the water populations could be assigned to water located in the cell wall, cytoplasmic water, and water in the vacuole (with the longest T_2 relaxation value) [40, 41]. In potato cells, another proton population with the lowest T2 relaxation value is evident, and it can be assigned to water on the surface or inside starch granules [42].

Changes in water NMR dynamic properties during ripening, processing, and storage operations on fruits and vegetables can, in principle, reveal sub-cellular modifications and contribute to a microscopic understanding of these processes [43]. Examples of the application of this approach are present in the literature [44–47].

A special kind of TD-NMR was applied in the present work, that is, the Mobile Universal Surface Explorer (Single-sided TD-NMR) [48, 49]. This portable, single-sided NMR device has been designed to evaluate the proton content of objects non-invasively and non-destructively. Specifically, we used it to measure the proton relaxation time and study the associated mobility of water molecules before and after the electroporation process on potato tissue samples of different varieties. Comparisons with apple tissue and preliminary measurements in a bulk TD-NMR instrument (Minispec) were also performed.

The T2 transverse relaxation times measured with the Single-sided TD-NMR were shown to be sensitive to the electroporation process. Preliminary studies with the NMR-Minispec and microscope observations confirmed the data and suggested a deeper comprehension of the process at the subcellular level.

2. Materials and Methods

Four different types of potato tubers, P1, P2, P3, and P4, and one type of apple were purchased from the local market. These different types of potato tubers belong to different varieties with clear or red peel and yellow core among those available at the experiments' time. The apple variety was the one available at the time of the experiment. The experiments were conducted in July. Each vegetable sample, either electroporated or non-electroporated, was analyzed using the Single-sided TD-NMR. Each side of the treated sample was analyzed to verify if the electroporation produced differences in terms of the water molecule’s mobility on the surface. The same analysis was applied to the non-electroporated samples to determine the differences by comparison.

For each sample type, the relaxation time T2 was also measured in the bulk instrument Minispec to better understand the Single-sided TD-NMR results.

Electroporated tissues were prepared for optical microscope visualization. Treated samples were observed one hour after electroporation. For each piece, both sides, top, and bottom were sliced and observed under a microscope to evaluate the cell membrane morphology. Non-treated pieces were also analyzed with the microscope for comparison.

24 h after treatment, the treated samples were observed for any color change and other electroporation effects.

2.1. Electroporation.

From each of the potato and apple, six parallelepiped pieces with a size close to 5 x 10 x 30 mm were cut. Three of the pieces were treated with the electroporation voltage pulses, and the other three were untreated controls. The voltage pulses were applied using the EPS02

voltage pulse generator (IGEA SpA, Carpi, MO, Italy) connected to a pair of parallel stainless steel plate electrodes with a gap of 5 mm, positioned, as shown in the set-up, in Fig. 1 (a) [50, 51].

To each sample, a sequence of 24 unidirectional voltage pulses, with a suitable amplitude in the order of 1000 V/cm (500 V) for potato and in the order of 2000 V/cm (1000 V) for apple tissue were applied to one of the 10 x 30 mm sides. For each sample, the area facing the positive electrode was marked. A and the one facing the negative electrode were marked B.

The two sides, the treated and the untreated one, were then analyzed using the SINGLE-SIDED TD-NMR probe. Finally, the sample's two sides were sliced, dyed with Methylene Blue, and observed at the optical microscope. The data of the electroporated samples were compared with those of the non-electroporated tissues.

2.2. Water content.

For each sample, the water content was measured by drying the samples in a static oven (Mod. 2100 High-Performance Oven, F.lli Galli) according to the following procedure: (i) three samples of the same vegetable was cut; (ii) each sample was weighed (HR-200 Scientific Balance, A&D Instruments), obtaining the value, m_{fresh}; (iii) the samples were dried for 24 h in a static oven at 100 °C; (iv) the same samples were weighted till constant weight, obtaining the dry weight, m_{dry}; (v) finally, the water content was computed as a percent using equation (1):

$$watercontent\ [\%] = 100\frac{m_{fresh}-m_{dry}}{m_{fresh}} \quad (4)$$

2.3. Tissue morphology.

The tissue morphology before and after electroporation was studied using an inverted microscope (Olympus IX50). A thin layer from each side of the potato and apple parallelepiped was cut in the electroporated area using a cutter. The larger section of the parallelepiped was chosen. The slices were washed using deionized water and immersed in 0.2% Methylene blue in deionized water (115943 Methylene blue C.I. 52015, Merck Chemicals) for 1 min. The pieces were washed again in deionized water and then placed on a microscope glass slide covered with a coverslip. Every slice was washed again by capillarity to remove the excess dye and was observed using an Olympus IX50 microscope with a magnification of 400× and a Canon EOS 1100D camera focusing on the cell membrane.

2.4. Single-sided TD-NMR vegetable tissue conductivity.

The vegetable tissue conductivity could be described as a non-linear function of the electric field intensity, σ(E), as in [50, 52]:

$$\sigma(E) = \sigma_0 + \frac{\sigma_1 - \sigma_0}{2}\left(1 + \tanh\left(k_v\left(E - E_{th}\right)\right)\right) \quad (5)$$

where σ_0 and σ_1 [S/m] is the conductivity at 0 V/cm, and at the maximum value of E (e.g., 1000 V/cm), respectively, k_v [m/V] is a constant and E_{th} [kV/m] is the electric field.

The electrical conductivity, σ, of the vegetable tissues was evaluated experimentally, using a suitable multi-box device, with 8 wells. Each well has a rectangular section (11x9 mm) and is 11.3 mm thick, as described in (Fig. 1 (b)). The voltage pulses were applied using a plate electrode formed by two stainless steel plates with rectangular geometry with the side 10 mm

long and distant L = 7 mm (covering all the box depth of 11.3 mm). The two plates were inserted into each box.

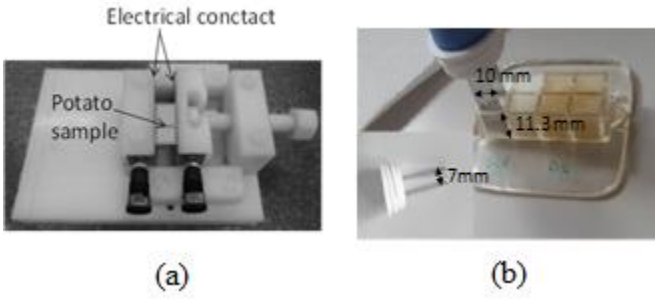

Figure 1. Experimental set-ups used for (a) the treatment with voltage pulses of the samples for the TD-NMR experiment and (b) for the evaluation of the electrical conductivity of the vegetable tissue [53].

Eight voltage pulses were applied to the electrode plates using the voltage pulse generator. The amplitude of the voltage pulses was varied from 100 V (E = 143 V/cm) to 1000 V (E = 1370 V/cm). Voltage and current values were recorded and analyzed to compute the resistance at the electrodes and the material's corresponding conductivity as in [30]. The conductivity was computed using Ohm's law in equation (3), and the model for the conductivity, σ, of a parallelepiped with section A = 10x11.3 mm and length L = 7 mm:

$$\sigma = \frac{1}{R}\frac{L}{A} \qquad (6)$$

The measured conductivity values as a function of the electric field intensity were fitted using the non-linear least mean square method to find the parameters of equation (2) [50, 54].

2.5. TD-NMR.

T_2 measurements were carried out using a Bruker compact spectrometer (Minispecmq-series). When equipped with a Profiler with a 0 mm depth probe, the single-sided TD-NMR surface has a Larmor frequency of 15.50 MHz. The samples were analyzed at room temperature using a multi-echo CPMG-type pulse sequence with echo times of 100 μs; 2500 echoes were recorded [55, 56]. For bulk T_2 measurements, the Bruker Minispec magnet was equipped with a 10 mm temperature-controlled probe with 6 μs dead time. The magnetic field strength was 0.47 T, corresponding to a resonance frequency for protons of 19.95 MHz. The samples were analyzed at 22 °C, using the Carr-Purcell-Meiboom-Gill (CPMG) sequence with a τ value of 150 μs. Data from 10000 echoes were acquired for 16 or 32 scans for each measurement.

The relaxation times of the different components were extracted from multiexponential decay curves using the program Uniform PENalty (UPEN), based on the inverse Laplace transform developed by Fantazzini and co-workers (Upenwin ver. 1.04) [57, 58].

UPEN inverts the CPMG signal searching for the least biased distribution of relaxation times according to the following equation: $I(2\tau n)=\Sigma i\ I_0(T_{2,i})\exp(-2\tau n/T_{2,i})$, where 2τ is the CPMG interpulse spacing, n is the index of a CPMG echo, and $I_0(T_{2,i})$ is the signal intensity of the $T_{2,i}$ component at τ= 0, sampled logarithmically in the interval between $T_{2,min}$ and $T_{2,max}$.Negative feedback is also applied by the software algorithm to a smoothing function to prevent excessive details in the distribution of relaxation times. As a consequence, the resolution of features is lowered as a default [59]. The major advantage of this approach concerning other fitting models (such as the Levenberg–Marquardt one) is that an a priori knowledge about the number of T_2s is unnecessary.

In the present work, the default UPEN parameters were generally adopted.

2.6. Statistical analysis.

Statistical analysis on measurements data was performed using an ANOVA test to compare the values of the relevant peaks of the T_2 time measured in different conditions.

3. Results and Discussion

Fig. 2 (a) and (b) show the non-electroporated tissue of a potato tuber. Here, arrow '1' points to the cell wall of a typical potato cell with polygonal shape, arrow '2' to the starch granules, and arrow '3' to an area where the cells are smaller and packed, and the white star represents the vacuole structure inside the cell. Differences in the tissue morphology (dimensions of cells and vacuoles or different starch granules packing) could cause differences in recorded values. It is well known that the potato tubers also show inhomogeneity in tissue morphology. Comparatively, the apple tissue is more homogeneous concerning potato tissue, and no starch granules are present, as shown in Fig. 2 (c).

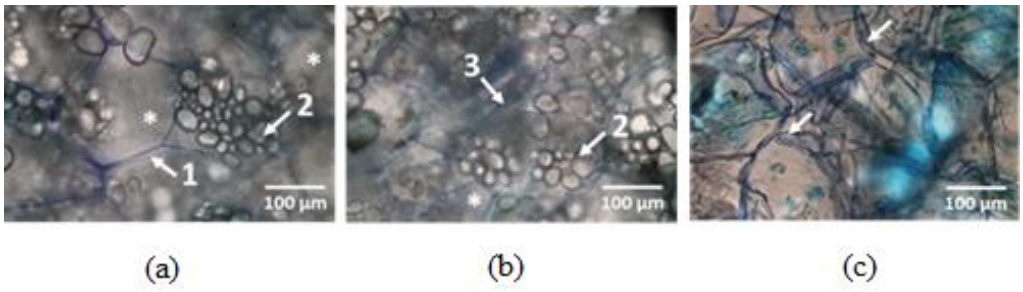

Figure 2. (a) and (b) Potato morphology for sample P1 (left) and P2 (right) and (c) apple tissue morphology. Stars identify the vacuole structure, where, arrow '1' shows the cell wall, arrow '2' shows the starch granules, and arrow 3 shows the area where the cells are smaller and packed.

To determine the electric field needed to electroporate the analyzed tissue's cell membrane, the sample conductivity was evaluated as in [24]. The electric field intensity was chosen to maximize conductivity and guarantee the tissue's electroporation for any higher field intensity.

The parameters of the curve of the vegetable tissue conductivity described in equation (2) as a function of the electric field intensity are obtained by fitting the measurement data obtained applying incremental voltage amplitude to potato or apple cube as described in Materials and Methods. The measured conductivities for each applied voltage for the four potato types and one apple are reported in Fig. 3 (a) and (b), respectively. Data obtained from the different potato samples are identified with different symbols (P1, crosses; P2, triangles; P3, circles; and P4, dots). Fig. 3(c) shows two examples of the treated potato samples 24 h after the treatment and the color changes due to electroporation, whereas Fig. 3(d) shows the apple samples treated with incremental electric field intensity observed 24 h after electroporation. The four different types of potatoes show differences in terms of conductivity. At an electric field of 1000 V/cm, all the potato tubers show their maximum conductivity values, indicating that the field intensity chosen to treat the potato slices analyzed with Single-sided TD-NMR is suitable to electroporate the tissues. In the case of the apple samples, the maximum conductivity is reached using an electric field intensity of 970 V/m; therefore, at 2000 V/cm, the electric field intensity used for the treatment of the apple slices analyzed with the Single-sided TD-NMR, the tissue could be considered electroporated.

The conductivity values measured in the experimental set-up in Fig. 1(b) and evaluated at each electric field amplitude are reported in Table 1, whereas Table 2A reports the values of the four parameters of the model (2) evaluated for each potato tuber or apple sample. Table 2B also reports the water content evaluated for each sample used in the experiments as determined by equation (1). The potatoes' water content was close to 80% in three of the samples, whereas the last potato tuber showed a higher value of 83%. The ANOVA analysis would have a p-value of 0.086 for all the potato tubers compared and a p-value of 0.27 if the P1, P2, and P3 samples were considered, indicating that the values are statistically not significantly different (p=0.05). Quantitatively, the samples P1, P2, and P3 have a comparable water content, whereas the water content of the sample P4 is higher. In apple samples, the water content was 83%.

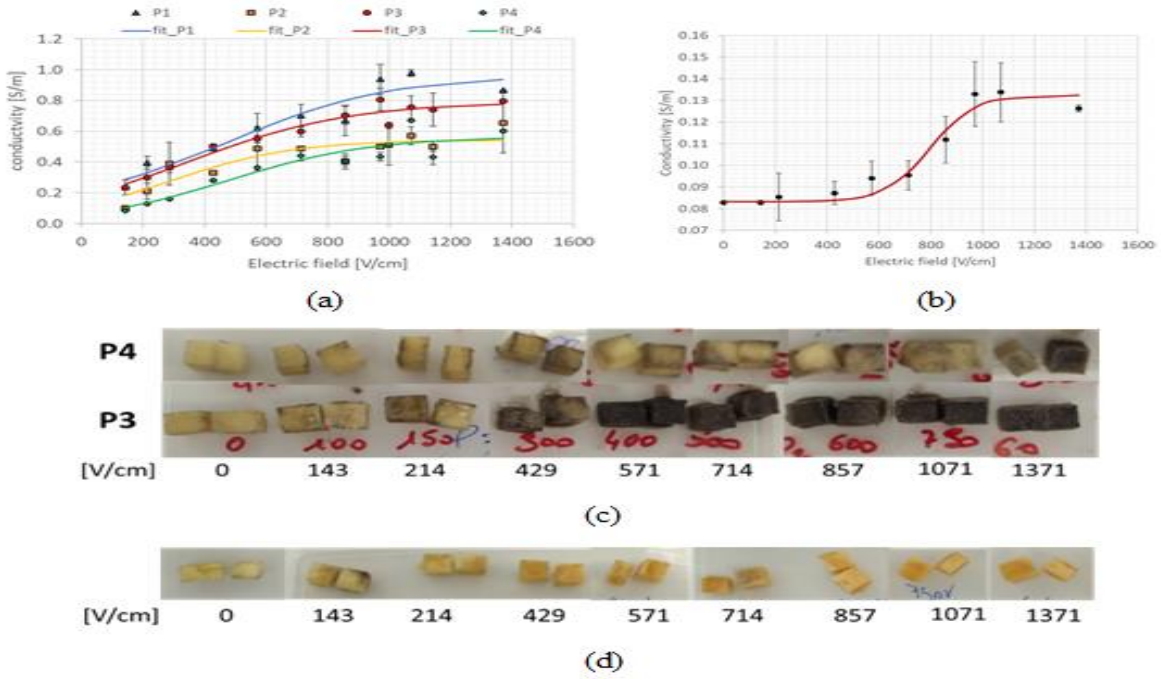

Figure 4. Conductivity in [S/m] as a function of the electric field amplitude in [V/cm] for (a) the four tubers analyzed and (b) apple tissue. (b) Pictures of the vegetable pieces electroporated at different electric field intensities taken 24 h after treatment: (c) two representative samples, P2 and P3, of potato tubers and (d) apple tissue.

Table 1. Conductivity in [S/m] measured at different electric field amplitudes in [V/cm] with standard deviation for potato and apple samples.

	P1		P2		P3		P4		A1	
E [V/cm]	σ [S/m] -	std (σ)	σ [S/m]	std (σ)	σ [S/m] -	std (σ)	σ [S/m] -	std (σ)	σ [S/m] -	std (σ)
143	0.23	±0.050	0.10	±0.017	0.23	±0.050	0.08	±0.000	0.083	±0.000
214	0.40	±0.043	0.21	±0.052	0.30	±0.074	0.13	±0.010	0.083	±0.000
429	0.49	±0.001	0.33	±0.012	0.50	±0.015	0.28	±0.011	0.087	±0.005
571	0.62	±0.096	0.49	±0.143	0.55	±0.024	0.36	±0.000	0.094	±0.008
714	0.70	±0.075	0.49	±0.000	0.60	±0.034	0.44	±0.033	0.095	±0.007
857	0.67	±0.098	0.41	±0.029	0.70	±0.059	0.40	±0.049	0.112	±0.011
971	0.94	±0.097	0.50	±0.005	0.81	±0.073	0.44	±0.028	0.133	±0.015
1071	0.98	±0.022	0.57	±0.059	0.76	±0.073	0.67	±0.004	0.134	±0.01
1371	0.87	±0.000	0.65	±0.194	0.80	±0.007	0.60	±0.010	0.126	±0.00

Table 2a. Values of the parameters of the conductivity model (2) for potato and apple samples.

Sample	σ_0 [S/m]	σ_1 [S/m]	k_v [cm/V]	E_{th} [kV/cm]
P1	0.104	0.96	0.0012	480.7
P2	0.0001	0.54	0.0024	280.9
P3	0.0001	0.79	0.0019	340.1
P4	0.0001	0.56	0.0021	478.2
A1	0.083	0.132	0.0058	797.1

Table 2b. Water content [%] for potato and apple samples.

Sample	Water content [%]	Std [%]
P1	79.4	±0.3
P2	79.5	±1.1
P3	80.6	±0.4
P4	83.0	±0.7
A1	83%	±0.7

The potato and apple tissues treated with the electric field observed 24 h after electroporation appear dark compared to the non-treated ones, which maintained their original yellow color. Fig. 4 shows the potato and apple pieces 24 h after pulse application. In potato samples, the color after electroporation is between dark brown and black. Specifically, the color change after electroporation of samples P1 and P2 is less intense than the one that occurred in samples P3 and P4. Electroporation of the apple sample caused the color to become clear brown from the original yellow of the non-electroporated sample.

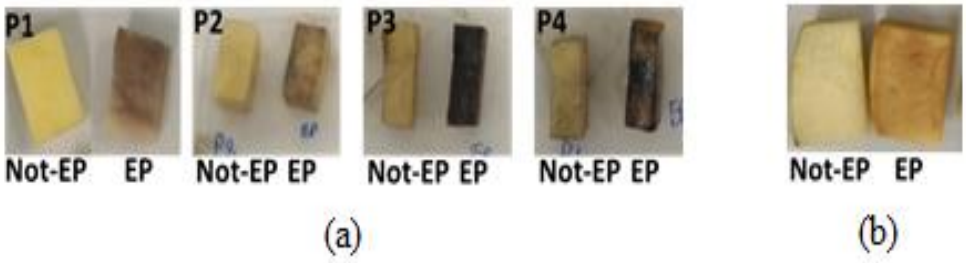

Figure 4. Vegetable pieces treated (labeled with EP) and non-treated were observed 24 h after the voltage pulses application. (a) potato, 4 tubers, and (b) apple.

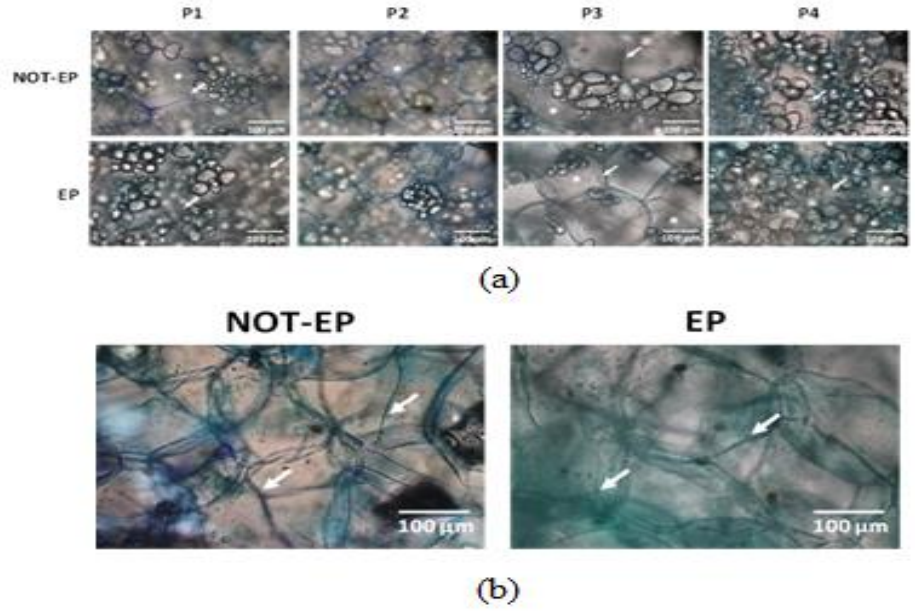

Figure 5. Microscope images of non-treated and electroporated (a) potato (4 tubers) and (b) for apple tissue. Arrows highlight membrane and cell wall, while stars the vacuole structure.

At the microscopic level, the images of the potato tissue (Fig.5 (a)) reveal well-defined cell membranes and cell walls, with a regular and square shape in the non-treated tissues, whereas they appear damaged and with an irregular shape in the electroporated tissue[60–65]. Here, the arrow in the electroporated samples (EP) shows the points where the cell membrane appears detached from the cell wall. In the non-electroporated samples' images, the cell membrane appears attached to the cell wall and shows a regular shape. The stars in both series

of images show vacuole structures that are retracted in the electroporated cells. This could be related to the loss of liquid fraction. The tissue after electroporation shows a larger loss of liquid less than the one related to non-treated tissue observed at the same time. Fig. 5 (b) shows a comparison of the apple tissues before and after electroporation. In this case, the cell wall, marked with white arrows, is modified; cells appear to be of irregular shape, and the cell membrane detached from the cell wall.

Fig. 6 shows the Single-Sided TD-NMR T_2 values follow the typical distribution. The peak component at 150-160 ms and a broader one in the range 0.5-20 ms could be identified in all the samples, both treated and non-treated. The arrow with the star marks the 150-160 ms component. Comparing with the T_2 profiles reported in the literature, we can assign the main peak to the water in the vacuole marked by the arrow on the right side (water in the vacuole shows the longest T_2 value), and the other water populations are overlapped. The left two arrows indicate the contribution of water, not in vacuole towards T2. Specifically, the water populations could be assigned to water located on the cell wall, cytoplasmatic water, and water linked to starch granules [41–43].

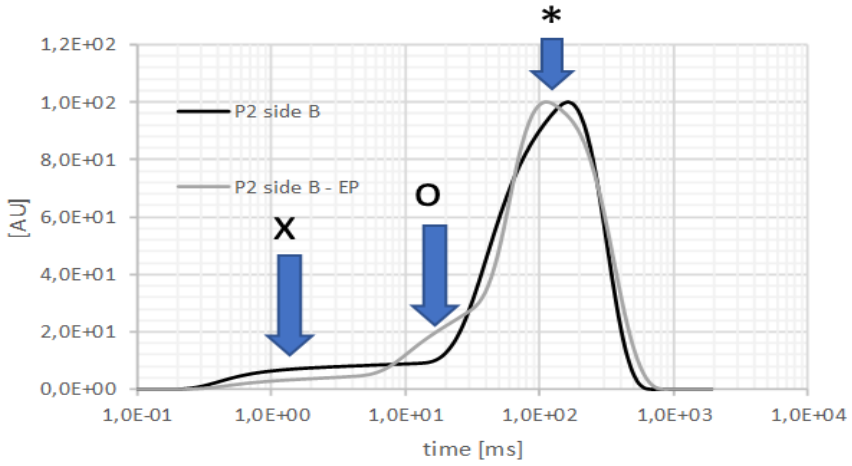

Figure 6. Typical inverse Laplace transform of the T2 signal for not-treated and treated potatoes, where the main peak is marked by the star and the other water components are marked by a cross and a circle.

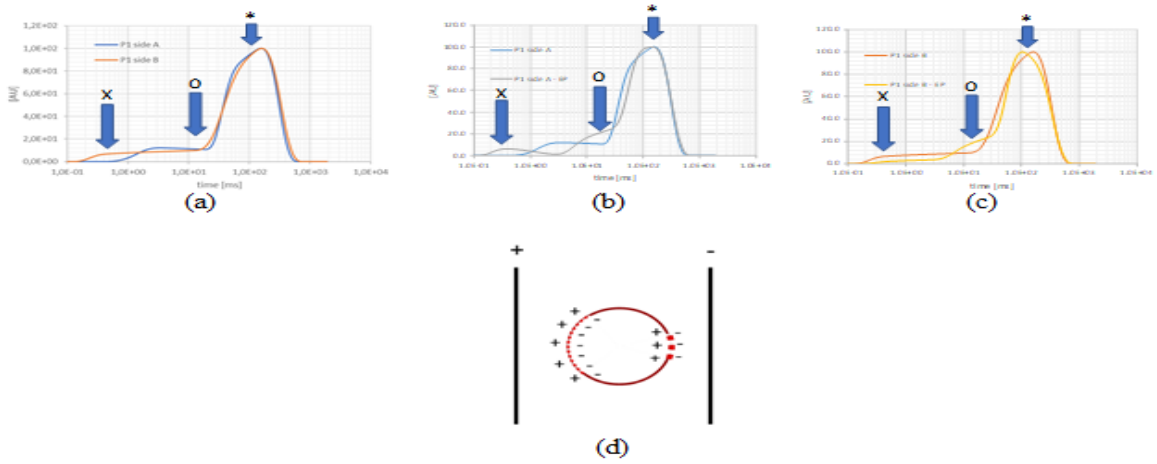

Figure 7. inverse Laplace transform of the T2 signal (a) for not-treated potato side A and B and for electroporated and non-electroporated potato (b) side A and (c) side B. Panel (d) represents the electroporation asymmetry if unipolar pulses are used.

In Fig. 6, the T2 relaxation value behavior at sides A and B of the sample is also reported. The T_2 values show a difference in the area marked by the two arrows at the left. In fact, it is well known that the electroporation effect is different on the side facing the positive

and the negative electrode if the pulses are applied in the same direction without reversing them periodically [11].

It must be noted that, due to the inhomogeneous magnetic field of the Single-sided TD-NMR, the T_2 values measured in this work are shorter than the values previously reported for homogeneous TD-NMR, but some similar considerations apply.

In the case of electroporated potatoes, the first part of the profile changes, and the T_2 relaxation value of the main population is lower.

Fig.7a-c shows the T_2 distribution evaluated at side A and side B of electroporated and non-electroporated potato slices. In the non-treated potato, side A and B show a similar profile, whereas side A and B display differences in T2 distribution for the electroporated potato. The observed asymmetry could be related to the opposite polarity of the electrodes on the two sides as schematically represented in Fig 7 (d), where the side facing the positive electrode shows a larger electroporated area on the membrane surface with smaller pores, whereas on the side facing the negative electrode the electroporation area is smaller, but with larger pores [11]. Finally, considering electroporated samples, the area's peak marked a circle appears modified concerning both the signal related to the non-electroporated sample (side A and side B).

In Table 3, the values of the main T_2 component for each side of the electroporated and non-electroporated potato pieces are reported. Both sides of non-electroporated potatoes show the same T_2 values. The electroporated pieces' peak maxima are shifted toward lower values, and the two sides of the electroporated potato show different peak shifts. The T_2 of the positive side (A) is longer than the negative one (B). This result reflects the asymmetry of the electroporation process. The electroporation of cell membranes depends on the voltage polarity of the applied pulses. The side of the membrane facing a positive polarity shows a larger area of electroporation, whereas the side of the cell membrane facing the zero voltage electrode (negative polarity) experiments more intense electroporation in a smaller area, as shown in Fig. 7(b)-(c) [66]. Because the Single-sided TD-NMR detects water in the first layer (up to a maximum depth of 1 mm), it can distinguish the two sides.

Table 3. Position of the main peak [ms] in electroporated and non-electroporated potatoes.

	Side A	**Side B**	**EP Side A**	**EP Side B**
P1	156	159	143	105
P2	162	162	166	113
P3	150	180	138	104
P4	156	151	139	134

Focusing on the values of the T_2 main peak for the non-electroporated sides (columns 1 and 2) in Table 3 and using ANOVA, it appears that the two groups are homogenous (the p-value is 0.32, null hypothesis: T_2 values for side A and side B are similar). Considering the electroporated side A of the potato piece and the corresponding non-electroporated one, the ANOVA analysis shows that the two groups are different (except for sample P2) and the p-value is < 0.05; nevertheless, the largest difference is observed on side B comparing the electroporated and the non-electroporated samples. In this case, the ANOVA analysis for the two groups of values shows a p-value <0.05 (0.001). Sides A and B analyzed after electroporation show a difference in T_2 value (p-value <0.05 – null hypothesis: T_2 values for side A and side B are similar). This result enforces the hypothesis that the electroporation in unipolar pulses is different if the slice surface is faced with the positive or negative electrode.

The potato sample P2 was also analyzed in the more homogeneous magnetic field of the Minispec instrument (Fig. 8a). The measured T_2 bulk values were different: the T_2 of the

vacuole population protons before and after electroporation 765.2 ms and 433.8 ms. A fast relaxing component (2.58 ms) is present. In the presence of a strongly inhomogeneous magnetic field, such as in the case of the Single-sided TD-NMR, the transverse relaxation time does not depend only on spin-spin interactions, but it is also controlled by molecular diffusion through the gradient, which results in a more rapid loss of coherence with the consequent shortening of the observed T_2 values and the disappearance of very short T_2 components. In potato cells, the lowest T_2 relaxation value can be assigned to water on the surface or inside starch granules [43]. Water in the cytoplasm, on cell walls, and in extracellular spaces shows overlapping T_2 values between 30-40 ms and 250-300 ms.

Electroporation causes a decrease of the T_2 value associated with the vacuole water protons, as observed in surface T_2 measurements. Starch water protons T_2 values appear as a more disperse component, with a maximum T_2 shifted to about 4.6 ms.

After drying the potato in the oven, only the starch protons T_2 component is still present (Fig. 8b), confirming the right attribution of the lowest T_2 value to this cell compartment.

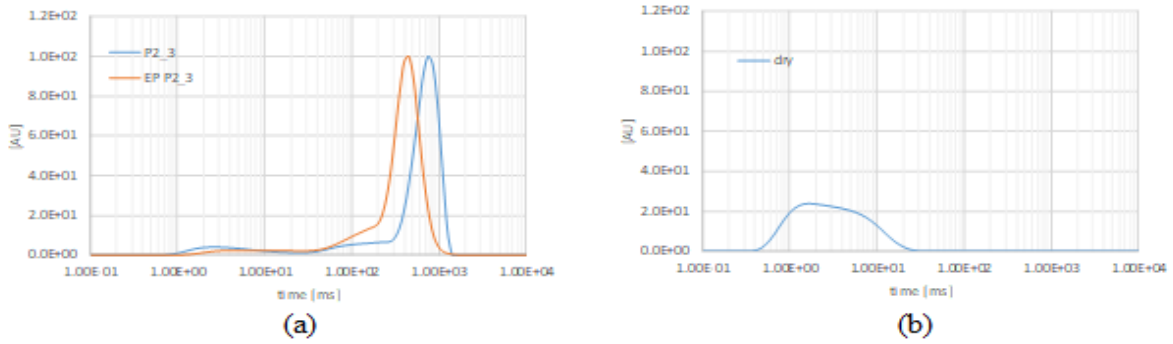

Figure 8. (a) T2 distribution of potato P2 before and after electroporation as measured with Minispec (b) T2 distribution in potato P2 after drying in the oven.

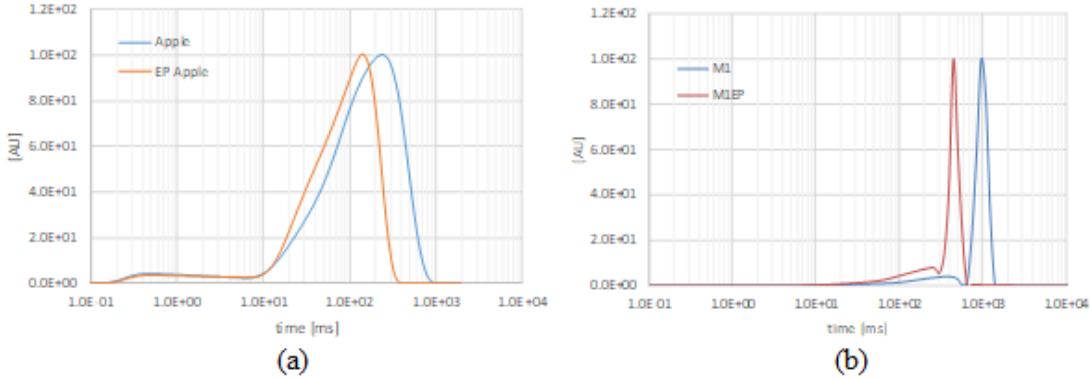

Figure 9. T2 distribution of the apple sample as measured with the Single-sided TD-NM0052 (a) and the Minispec (b).

NMR measurements on apple samples gave similar results to potato tissues. Fig 9a shows the T_2 distributions obtained before and after electroporation of apple with the Single-sided TD-NMR (side B) and Fig. 9b, with the Minispec. Using the Single-sided TD-NMR, the longest T_2 value (237.6 ms) is higher than the one found in potatoes. This could be, probably because apples have bigger vacuoles than potatoes. Similar to what was found with potatoes, after electroporation, this peak is shifted to lower values (141.4 ms).

As expected, T_2 values in a more homogeneous field are higher than in the inhomogeneous Single-sided TD-NMR. Water protons in vacuoles have a T_2 relaxation time

of 992.9 ms, while after electroporation, the value decreases to 792.8 ms. In comparison with potato proton populations, the absence of starch protons T_2 component is evident. Correlations of T_2 values with vacuolar volumes and water loss were already reported in the literature [39, 42].

4. Conclusions

In this research, changes in potato tubers and apple tissues treated with electroporation were studied, evaluating the tissues' conductivity, taking microscope images, and analyzing their TD-NMR response.

The analysis using TD-NMR shows different behaviors in the distribution of the transverse relaxation time T_2 values. The differences could be related to the modification in the structure of the cells that were damaged by voltage pulses and consequently lost some water originally stored inside their structure. This loss of internal water was also visible at a macroscopic level observing that the electroporated slices were wetter than the non-treated ones.

The T_2 differences in treated and non-treated samples observed in this work may be explained with increased permeability of water pools across membranes due to the electroporation that affected the exchange rate among water protons from different compartments and leads to a loss of vacuolar water content.

The vacuole size reduction has been initially evidenced by decreasing the main T_2 value at the portable Single-sided TD-NMR and by the acquisition of images obtained at the electronic microscope.

A more accurate analysis of the transverse relaxation time distribution in potato and apple was performed using TD-NMR Minispec to confirm the relationship between the T_2 values and the different compartments of the cells in which water is found. Moreover, the Minispec data of potato samples showed an interesting increase in the T2 value associated with the starch granules' protons upon electroporation. This can be explained by increased mobility of the starch in the cytoplasm after reducing the vacuolar volume.

Overall, comparing all the data obtained in the present work, TD-NMR's ability in monitoring subcellular water compartmentation proved to be valuable to confirm the cell changes after the electroporation process quickly, and there is a good correlation with previous literature.

Funding

This research received no external funding.

Acknowledgments

Roberta Bertani and MirtoMozzon wish to thank the TWINNING-2017 research project “Supramolecular transition-metal architectures based on non-covalent interactions for selective molecular sorption and non-linear optics: Rational design and preparation” of the Industrial Engineering Department (University of Padova) for the financial support. The authors are also grateful to Igea spa, Carpi (MO), Italy, for the pulse generator loan

Conflicts of Interest

The authors declare no conflict of interest.

References

1. Kotnik, T.; Kramar, P.; Pucihar, G.; Miklavčič, D.; Tarek, M. Cell membrane electroporation - Part 1: The phenomenon. *IEEE Elect Insul Mag* **2012**, *28*, 14–23, https://doi.org/10.1109/MEI.2012.6268438.
2. Zimmermann, U.; Pilwat, G.; Riemann, F. Dielectric breakdown of cell membranes. *Biophy J* **1974**, *14*, 881–899, https://dx.doi.org/10.1016%2FS0006-3495(74)85956-4.
3. Kotnik, T.; Rems, L.; Tarek, M.; Miklavčič, D. Membrane Electroporation and Electropermeabilization: Mechanisms and Models. *Annu Rev Biophys* **2019**, *48*, 63-91, https://doi.org/10.1146/annurev-biophys-052118-115451.
4. Kiełbik, A.; Szlasa, W.; Saczko, J.; Kulbacka, J. Electroporation-Based Treatments in Urology. *Cancers (Basel)* **2020**, *12*, https://doi.org/10.3390/cancers12082208.
5. Sherba, J.J.; Hogquist, S.; Lin, H.; Shan, J.W.; Shreiber, D.I.; Zahn, J.D. The effects of electroporation buffer composition on cell viability and electro-transfection efficiency. *Scientific Reports* **2020**, *10*, 3053, 1-9. https://doi.org/10.1038/s41598-020-59790-x.
6. Cao, Y.; Ma, E.; Cestellos-Blanco, S.; Zhang, B.; Qiu, R.; Su, Y.; Doudna, J.A.; Yang, P. Nontoxic nanopore electroporation for effective intracellular delivery of biological macromolecules. *Proceedings of the National Academy of Sciences* **2019**, *116*, 7899-7904, https://doi.org/10.1073/pnas.1818553116.
7. Sachdev, S.; Feijoo Moreira, S.; Keehnen, Y.; Rems, L.; Kreutzer, M.T.; Boukany, P.E. DNA-membrane complex formation during electroporation is DNA size-dependent. *Biochimica et Biophysica Acta (BBA) - Biomembranes* **2020**, *1862*, https://doi.org/10.1016/j.bbamem.2019.183089.
8. Tivig, I.; Savopol, T.; Kovacs, E.; Moisescu, M.G. An experimental system for real-time fluorescence recordings of cell membrane changes induced by electroporation. *European biophysics journal* **2020**, *49*, 105-111, https://doi.org/10.1007/s00249-019-01417-9.
9. Hoejholt, K.L.; Mužić, T.; Jensen, S.D.; Dalgaard, L.T.; Bilgin, M.; Nylandsted, J.; Heimburg, T.; Frandsen, S.K.; Gehl, J. Calcium electroporation and electrochemotherapy for cancer treatment: Importance of cell membrane composition investigated by lipidomics, calorimetry and in vitro efficacy. *Scientific Reports* **2019**, *9*, 1-12, https://doi.org/10.1038/s41598-019-41188-z.
10. Wu, Y.; Fu, A.; Yossifon, G. Active particles as mobile microelectrodes for selective bacteria electroporation and transport. *Sci Adv* **2020**, *6*, https://doi.org/10.1126/sciadv.aay4412.
11. Leontiadou, H.; Mark, A.E.; Marrink, S.J. Molecular dynamics simulations of hydrophilic pores in lipid bilayers. *Biophys J* **2004**, *86*, 2156-2164, https://doi.org/10.1016/S0006-3495(04)74275-7.
12. Rols, M.-P. Mechanism by Which Electroporation Mediates DNA Migration and Entry into Cells and Targeted Tissues. In: *Electroporation Protocols: Preclinical and Clinical Gene Medicine*. Li, S.; Ed. Humana Press: Totowa, NJ, **2008;** pp. 19-33, https://doi.org/10.1007/978-1-59745-194-9_2.
13. Joshi, R.P.; Hu, Q.; Aly, R.; Schoenbach, K.H.; Hjalmarson, H.P. Self-consistent simulations of electroporation dynamics in biological cells subjected to ultrashort electrical pulses. *Physical review. E, Statistical, non-linear, and soft matter physics* **2001**, *64*, https://doi.org/10.1103/PhysRevE.64.011913.
14. Probst, U.; Fuhrmann, I.; Beyer, L.; Wiggermann, P. Electrochemotherapy as a New Modality in Interventional Oncology: A Review. *Technology in cancer research & treatment* **2018**, *17*, https://doi.org/10.1177/1533033818785329.
15. Marty, M.; Sersa, G.; Garbay, J.R.; Gehl, J.; Collins, C.G.; Snoj, M.; Billard, V.; Geertsen, P.F.; Larkin, J.O.; Miklavcic, D.; Pavlovic, I.; Paulin-Kosir, S.M.; Cemazar, M.; Morsli, N.; Soden, D.M.; Rudolf, Z.; Robert, C.; O'Sullivan, G.C.; Mir, L.M. Electrochemotherapy – An easy, highly effective and safe treatment of cutaneous and subcutaneous metastases: Results of ESOPE (European Standard Operating Procedures of Electrochemotherapy) study. *European Journal of Cancer Supplements* **2006**, *4*, 3-13, https://doi.org/10.1016/j.ejcsup.2006.08.002.
16. Ivorra, A.; Al-Sakere, B.; Rubinsky, B.; Mir, L.M. In vivo electrical conductivity measurements during and after tumor electroporation: conductivity changes reflect the treatment outcome. *Physics in medicine and biology* **2009**, *54*, 5949-5963, https://doi.org/10.1088/0031-9155/54/19/019.
17. Miklavčič, D. *Handbook of Electroporation*. **2016**.
18. Rebersek, M.; Miklavcic, D.; Bertacchini, C.; Sack, M. Cell membrane electroporation-Part 3: the equipment. *IEEE Electrical Insulation Magazine* **2014**, *30*, 8-18, https://doi.org/10.1109/MEI.2014.6804737.
19. Sampedro, F.; Rodrigo, D. Pulsed Electric Fields (PEF) Processing of Milk and Dairy Products. In: *Emerging Dairy Processing Technologies. Opp Dai Ind* **2015**; pp. 115–148, https://doi.org/10.1002/9781118560471.ch5.
20. Zhao, W.; Tang, Y.; Lu, L.; Chen, X.; Li, C. Review: Pulsed Electric Fields Processing of Protein-Based Foods. *Food and Bioprocess Technology* **2014**, *7*, 114-125, https://doi.org/10.1007/s11947-012-1040-1.
21. Mir, L.M.; Glass, L.F.; Sersa, G.; Teissié, J.; Domenge, C.; Miklavcic, D.; Jaroszeski, M.J.; Orlowski, S.; Reintgen, D.S.; Rudolf, Z.; Belehradek, M.; Gilbert, R.; Rols, M.P.; Belehradek, J., Jr.; Bachaud, J.M.; DeConti, R.; Stabuc, B.; Cemazar, M.; Coninx, P.; Heller, R. Effective treatment of cutaneous and

subcutaneous malignant tumours by electrochemotherapy. *British journal of cancer* **1998**, *77*, 2336-2342, https://doi.org/10.1038/bjc.1998.388.
22. Saulis, G. Electroporation of Cell Membranes: The Fundamental Effects of Pulsed Electric Fields in Food Processing. *Food Engineering Reviews* **2010**, *2*, 52-73, https://doi.org/10.1007/s12393-010-9023-3.
23. Donsì, G.; Ferrari, G.; Pataro, G. Inactivation kinetics of Saccharomyces cerevisiae by pulsed electric fields in a batch treatment chamber: The effect of electric field unevenness and initial cell concentration. *Journal of Food Engineering* **2007**, *78*, 784-792, https://doi.org/10.1016/j.jfoodeng.2005.11.027.
24. Toepfl, S.; Heinz, V.; Knorr, D. High intensity pulsed electric fields applied for food preservation. *Chemical Engineering and Processing: Process Intensification* **2007**, *46*, 537-546, https://doi.org/10.1016/j.cep.2006.07.011.
25. Eveke, D.J.G.; Brunkhorst, C. Inactivation of in Apple Juice by Radio Frequency Electric Fields. *Journal of Food Science* **2006**, *69*, FEP134-FEP0138, https://doi.org/10.1111/j.1365-2621.2004.tb13366.x.
26. Zhang, Q.; Monsalve-GonzÁLez, A.; Qin, B.-L.; Barbosa-CÁNovas, G.V.; Swanson, B.G. Inactivation Of Saccharomyces Cerevisiae In Apple Juice By Square-Wave And Exponential-Decay Pulsed Electric Fields. *Journal of Food Process Engineering* **1994**, *17*, 469-478, https://doi.org/10.1111/j.1745-4530.1994.tb00350.x.
27. Bertram, H.C.; Purslow, P.P.; Andersen, H.J. Relationship between Meat Structure, Water Mobility, and Distribution: A Low-Field Nuclear Magnetic Resonance Study. *J Agric Food Chem* **2002**, *50*, 824-829, https://doi.org/10.1021/jf010738f.
28. Proietti, N.; Adiletta, G.; Russo, P. Evolution of physicochemical properties of pear during drying by conventional techniques, portable-NMR, and modelling. *Journal of Food Engineering* **2018**, *230*, 82–98, https://doi.org/10.1016/j.jfoodeng.2018.02.028.
29. Menegazzo, I.; Mammi, S.; Sgarbossa, P.; Bartolozzi, A.; Mozzon, M.; Bertani, R.; Forzan, M.; Sundararajan, R.; Sieni, E. Time Domain Nuclear Magnetic Resonance (TD-NMR) to evaluate the effect of potato cell membrane electroporation. *Innovative Food Science & Emerging Technologies* **2020**, *65*, https://doi.org/10.1016/j.ifset.2020.102456.
30. Besghini, D.; Mauri, M.; Simonutti, R. Time Domain NMR in Polymer Science: From the Laboratory to the Industry. *Applied Sciences* **2019**, *9*, https://doi.org/10.3390/app9091801.
31. Nikolskaya, E.; Hiltunen, Y. Time-Domain NMR in Characterization of Liquid Fuels: A Mini-Review. *Energy & Fuels* **2020**, *34*, 7929-7934, https://doi.org/10.1021/acs.energyfuels.0c01464.
32. Tang, Y.; McCowan, D.; Song, Y.-Q. A miniaturized spectrometer for NMR relaxometry under extreme conditions. *Scientific Reports* **2019**, *9*, 1-9, https://doi.org/10.1038/s41598-019-47634-2.
33. Relaxation NMR. Available online: https://www.imaios.com/en/e-Courses/e-MRI/NMR/Relaxation-nmr (accessed on 7 Jan **2021**).
34. Parenti, O.; Guerrini, L.; Zanoni, B.; Marchini, M.; Tuccio, M.G.; Carini, E. Use of the 1H NMR technique to describe the kneading step of wholewheat dough: The effect of kneading time and total water content. *Food Chemistry* **2021**, *338*, https://doi.org/10.1016/j.foodchem.2020.128120.
35. Crook, A.A.; Powers, R. Quantitative NMR-Based Biomedical Metabolomics: Current Status and Applications. *Molecules* **2020**, *25*, https://doi.org/10.3390/molecules25215128.
36. Smits, J.; Damron, J.T.; Kehayias, P.; McDowell, A.F.; Mosavian, N.; Fescenko, I.; Ristoff, N.; Laraoui, A.; Jarmola, A.; Acosta, V.M. Two-dimensional nuclear magnetic resonance spectroscopy with a microfluidic diamond quantum sensor. *Science Advances* **2019**, *5*, https://doi.org/10.1126/sciadv.aaw7895.
37. Bartusik-Aebisher, D.; Aebisher, D.; Czmil, M.; Mazur, D. Evaluation of MR relaxation times following trastuzumab treatment of breast cancer cells in a 3D bioreactor. *Acta Poloniae Pharmaceutica - Drug Research* **2020**, *77*, 35-41, https://doi.org/10.32383/appdr/115519.
38. Sorte, E.G.; Rimsza, J.M.; Alam, T.M. Computational and Experimental 1H-NMR Study of Hydrated Mg-Based Minerals. *Molecules* **2020**, *25*, https://doi.org/10.3390/molecules25040933.
39. Lin, X.; Zhan, H.; Li, H.; Huang, Y.; Chen, Z. NMR Relaxation Measurements on Complex Samples Based on Real-Time Pure Shift Techniques. *Molecules* **2020**, *25*, https://doi.org/10.3390/molecules25030473.
40. Duynhoven, J.; Voda, M.; Witek, M.; As, H. Time-Domain NMR Applied to Food Products. *Annual Reports on NMR Spectroscopy* **2010**, *69*, 145-197, https://doi.org/10.1016/S0066-4103(10)69003-5.
41. Snaar, J.E.M.; Van As, H. Probing water compartments and membrane permeability in plant cells by 1H NMR relaxation measurements. *Biophys J* **1992**, *63*, 1654-1658, https://doi.org/10.1016/S0006-3495(92)81741-1.
42. Hills, B.P.; Remigereau, B. NMR studies of changes in subcellular water compartmentation in parenchyma apple tissue during drying and freezing. *International Journal of Food Science & Technology* **1997**, *32*, 51-61, https://doi.org/10.1046/j.1365-2621.1997.00381.x.
43. Hansen, C.L.; Thybo, A.K.; Bertram, H.C.; Viereck, N.; van den Berg, F.; Engelsen, S.B. Determination of Dry Matter Content in Potato Tubers by Low-Field Nuclear Magnetic Resonance (LF-NMR). *J Agric Food Chem* **2010**, *58*, 10300-10304, https://doi.org/10.1021/jf101319q.
44. Capitani, D.; Sobolev, A.P.; Delfini, M.; Vista, S.; Antiochia, R.; Proietti, N.; Bubici, S.; Ferrante, G.; Carradori, S.; De Salvador, F.R.; Mannina, L. NMR methodologies in the analysis of blueberries. *Electrophoresis* **2014**, *35*, 1615-1626, https://doi.org/10.1002/elps.201300629.

45. Capitani, D.; Mannina, L.; Proietti, N.; Sobolev, A.P.; Tomassini, A.; Miccheli, A.; Di Cocco, M.E.; Capuani, G.; De Salvador, R.; Delfini, M. Monitoring of metabolic profiling and water status of Hayward kiwifruits by nuclear magnetic resonance. *Talanta* **2010**, *82*, 1826-1838, https://doi.org/10.1016/j.talanta.2010.07.080.
46. Raffo, A.; Gianferri, R.; Barbieri, R.; Brosio, E. Ripening of banana fruit monitored by water relaxation and diffusion 1H-NMR measurements. *Food Chemistry* **2005**, *89*, 149-158, https://doi.org/10.1016/j.foodchem.2004.02.024.
47. Imakumbili, M.L.E.; Semu, E.; Semoka, J.M.R.; Abass, A.; Mkamilo, G. Plant tissue analysis as a tool for predicting fertiliser needs for low cyanogenic glucoside levels in cassava roots: An assessment of its possible use. *PLoS One* **2020**, *15*, https://doi.org/10.1371/journal.pone.0228641.
48. Blümich, B.; Perlo, J.; Casanova, F. Mobile single-sided NMR. *Prog Nuc Mag Reson Spect* **2008**, *52*, 197–269, https://doi.org/10.1016/j.pnmrs.2007.10.002.
49. Capitani, D.; Sobolev, A.P.; Di Tullio, V.; Mannina, L.; Proietti, N. Portable NMR in food analysis. *Chemical and Biological Technologies in Agriculture* **2017**, *4*, https://doi.org/10.1186/s40538-017-0100-1.
50. Bernardis, A.; Bullo, M.; Campana, L.G.; Di Barba, P.; Dughiero, F.; Forzan, M.; Mognaschi, M.E.; Sgarbossa, P.; Sieni, E. Electric field computation and measurements in the electroporation of inhomogeneous samples. *Open Physics* **2017**, *15*, 790-796, https://doi.org/10.1515/phys-2017-0092.
51. Bertacchini, C.; Margotti, P.M.; Bergamini, E.; Lodi, A.; Ronchetti, M.; Cadossi, R. Design of an irreversible electroporation system for clinical use. *Technology in cancer research & treatment* **2007**, *6*, 313-320, https://doi.org/10.1177/153303460700600408.
52. Breton, M.; Buret, F.; Krähenbühl, L.; Leguèbe, M.; Mir, L.; Perrussel, R.; Poignard, C.; Scorretti, R.; Voyer, D. Non-Linear Steady-State Electrical Current Modeling for the Electropermeabilization of Biological Tissue. *IEEE Transactions on Magnetics* **2015**, *51*, 1-4, https://doi.org/10.1109/TMAG.2014.2351836.
53. Campana, L.G.; Cesari, M.; Dughiero, F.; Forzan, M.; Rastrelli, M.; Rossi, C.R.; Sieni, E.; Tosi, A.L. Electrical resistance of human soft tissue sarcomas: an ex vivo study on surgical specimens. *Med Biol Eng Comput* **2016**, *54*, 773-787, https://doi.org/10.1007/s11517-015-1368-6.
54. Sarnago, H.; Sieni, E.; Lopez-Alonso, B.; Carrctcro, C.; Burdio, J.M.; Ó, L. An Inter-Disciplinary Approach to Teaching Biomedical Electronics with an Electroporation-Applied Example. In: Proceedings of 2018 IEEE 27th International Symposium on Industrial Electronics (ISIE). 13-15 June **2018**; pp. 901-905.
55. Carr, H.Y.; Purcell, E.M. Effects of Diffusion on Free Precession in Nuclear Magnetic Resonance Experiments. *Physical Review* **1954**, *94*, 630-638, https://doi.org/10.1103/PhysRev.94.630.
56. Meiboom, S.; Gill, D. Modified Spin-Echo Method for Measuring Nuclear Relaxation Times. *Review of Scientific Instruments* **1958**, *29*, 688-691, https://doi.org/10.1063/1.1716296.
57. Borgia, G.C.; Brown, R.J.S.; Fantazzini, P. Uniform-Penalty Inversion of Multiexponential Decay Data: II. Data Spacing, T2 Data, Systematic Data Errors, and Diagnostics. *Journal of Magnetic Resonance* **2000**, *147*, 273-285, https://doi.org/10.1006/jmre.2000.2197.
58. Borgia, G.C.; Brown, R.J.S.; Fantazzini, P. Uniform-Penalty Inversion of Multiexponential Decay Data. *Journal of Magnetic Resonance* **1998**, *132*, 65-77, https://doi.org/10.1006/jmre.1998.1387.
59. Venditti, G.; Schievano, E.; Navarini, L.; Mammi, S. Water Mobility and Distribution in Green Coffee Probed by Time-Domain Nuclear Magnetic Resonance. *Food Biophysics* **2011**, *6*, 321-326, https://doi.org/10.1007/s11483-010-9194-8.
60. Ivorra, A.; Mir, L.M.; Rubinsky, B. Electric Field Redistribution due to Conductivity Changes during Tissue Electroporation: Experiments with a Simple Vegetal Model. In: Proceedings of World Congress on Medical Physics and Biomedical Engineering. September 7 - 12, 2009, Munich, Germany, Berlin, Heidelberg, **2010**; pp. 59-62.
61. Hjouj, M.; Rubinsky, B. Magnetic resonance imaging characteristics of nonthermal irreversible electroporation in vegetable tissue. *The Journal of membrane biology* **2010**, *236*, 137-146, https://doi.org/10.1007/s00232-010-9281-2.
62. Knorr, D.; Angersbach, A. Impact of high-intensity electric field pulses on plant membrane permeabilization. *Trends in Food Science & Technology* **1998**, *9*, 185-191, https://doi.org/10.1016/S0924-2244(98)00040-5.
63. Galindo, F.G.; Vernier, P.T.; Dejmek, P.; Vicente, A.; Gundersen, M.A. Pulsed electric field reduces the permeability of potato cell wall. *Bioelectromagnetics* **2008**, *29*, 296-301, https://doi.org/10.1002/bem.20394.
64. Angersbach, A.; Heinz, V.; Knorr, D. Electrophysiological model of intact and processed plant tissues: cell disintegration criteria. *Biotechnol Prog* **1999**, *15*, 753-762, https://doi.org/10.1021/bp990079f.
65. Angersbach, A.; Heinz, V.; Knorr, D. Effects of pulsed electric fields on cell membranes in real food systems. *Innovative Food Science & Emerging Technologies* **2000**, *1*, 135-149, https://doi.org/10.1016/S1466-8564(00)00010-2.
66. Gehl, J. Electroporation: theory and methods, perspectives for drug delivery, gene therapy and research. *Acta physiologica Scandinavica* **2003**, *177*, 437-447, https://doi.org/10.1046/j.1365-201X.2003.01093.x.